JACS
JOURNAL OF THE AMERICAN CHEMICAL SOCIETY

Article

pubs.acs.org/JACS

Imaging and Quantitation of a Succession of Transient Intermediates Reveal the Reversible Self-Assembly Pathway of a Simple Icosahedral Virus Capsid

María Medrano, Miguel Ángel Fuertes, Alejandro Valbuena, Pablo J. P. Carrillo, Alicia Rodríguez-Huete, and Mauricio G. Mateu*

Centro de Biología Molecular "Severo Ochoa" (CSIC-UAM), Universidad Autónoma de Madrid, 28049 Madrid, Spain

Supporting Information

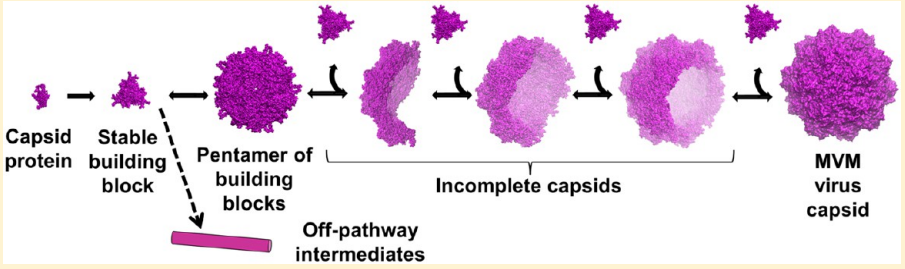

ABSTRACT: Understanding the fundamental principles underlying supramolecular self-assembly may facilitate many developments, from novel antivirals to self-organized nanodevices. Icosahedral virus particles constitute paradigms to study self-assembly using a combination of theory and experiment. Unfortunately, assembly pathways of the structurally simplest virus capsids, those more accessible to detailed theoretical studies, have been difficult to study experimentally. We have enabled the in vitro self-assembly under close to physiological conditions of one of the simplest virus particles known, the minute virus of mice (MVM) capsid, and experimentally analyzed its pathways of assembly and disassembly. A combination of electron microscopy and high-resolution atomic force microscopy was used to structurally characterize and quantify a succession of transient assembly and disassembly intermediates. The results provided an experiment-based model for the reversible self-assembly pathway of a most simple ($T = 1$) icosahedral protein shell. During assembly, trimeric capsid building blocks are sequentially added to the growing capsid, with pentamers of building blocks and incomplete capsids missing one building block as conspicuous intermediates. This study provided experimental verification of many features of self-assembly of a simple $T = 1$ capsid predicted by molecular dynamics simulations. It also demonstrated atomic force microscopy imaging and automated analysis, in combination with electron microscopy, as a powerful single-particle approach to characterize at high resolution and quantify transient intermediates during supramolecular self-assembly/disassembly reactions. Finally, the efficient in vitro self-assembly achieved for the oncotropic, cell nucleus-targeted MVM capsid may facilitate its development as a drug-encapsidating nanoparticle for anticancer targeted drug delivery.

INTRODUCTION

Virus self-assembly is eliciting great interdisciplinary interest from physical chemistry and biochemistry to nanoscience and nanotechnology, because it involves a complex yet efficient chain of molecular recognition events at the nanoscale.[1−5] Fundamental studies on the assembly of virus protein shells (capsids) are contributing to the understanding of supramolecular self-assembly and its relationship to biological function; the development of antiviral drugs that inhibit or misdirect virus assembly;[6,7] the efficient production and engineering of virus-like nanoparticles (VLPs) for biomedical or nanotechnological applications;[8−13] and the design of other self-assembling nanoparticles and nanomaterials.[14−19]

Spherical virus capsids are ubiquitous, and their relatively simple icosahedral architecture has encouraged the development of simplified theoretical models and coarse-grained simulations of their self-assembly. The influential thermodynamic-kinetic model by Zlotnick and collaborators and other models and simulations describe capsid assembly as a nucleation and growth process; they also predict specific assembly pathways through gradual association of capsid building blocks (CBBs), as well as quaternary structures of favored intermediate states.[1−3,5,20−32] Self-assembly of some icosahedral virus capsids in vitro[33,34] enabled experimental thermodynamics and kinetics studies of capsid assembly (see recent reviews[1−5] for references to in vitro studies with different viruses). The results obtained are generally consistent with predictions of different models and simulations (see reviews[1−3,5] and references therein), and/or provided constraints to develop or refine some models.

Received: July 25, 2016
Published: November 10, 2016

DOI: 10.1021/jacs.6b07663
J. Am. Chem. Soc. 2016, 138, 15385−15396

Unfortunately, the experimental investigation of pathways of assembly and disassembly for the simplest icosahedral virus capsids, those more accessible to detailed theoretical studies, has been hampered because these processes have frequently been observed as two-state reactions between free CBBs and complete capsids;[2,4,29] stable, populated intermediates were only rarely found.[35] However, considerable progress has been made in identifying or deducing the presence of scarcely populated, transient intermediates along the in vitro assembly or disassembly pathways of relatively simple icosahedral virus capsids, either in the absence or presence of other elements (scaffolding proteins and the viral nucleic acid).[36−53] In many cases, intermediates were stabilized relative to initial and/or final states through changes in biochemical conditions or genetic modifications in the viral proteins. Biophysical techniques to detect (dis)assembly intermediates for a variety of viruses[36−53] included electron microscopy (EM), size-exclusion chromatography (SEC), X-ray and neutron scattering, electrospray ionization-mass spectrometry (MS), ion-mobility-MS, hydrogen−deuterium exchange-MS, resistive-pulse sensing, etc.

Extremely valuable experimental information has thus been obtained on icosahedral capsid assembly or disassembly pathways, but several limiting aspects in the comparison with theoretical predictions have been noted: (i) Transient intermediates of in vitro assembly have been identified only for not so simple capsids with triangulation numbers $T \geq 3$, built from many (≥90) CBBs through conformational switches to achieve different (quasiequivalent) conformations of the capsid subunits. The simplest $T = 1$ capsids of some parvoviruses have been self-assembled in vitro,[54−56] but no thermodynamic or kinetic analyses were carried out. (ii) Some of the capsids studied are formed in vivo and in vitro in a coassembly process with either the viral nucleic acid or scaffolding proteins; some models and simulations of assembly contemplated these additional elements, but other relevant theoretical studies considered capsid proteins only. (iii) Some capsids for which the help of nucleic acid or scaffolding proteins are indispensable in vivo could be assembled in vitro without the help of these molecules, but nonphysiological conditions were frequently needed. (iv) Irreversible maturation steps that take place during in vivo assembly of many capsids were not contemplated in most models and simulations. (v) For the $T = 3$ Cowpea Chlorotic Mosaic Virus a comparison of assembly versus disassembly intermediates revealed a common intermediate, but also disassembly intermediates that were not identified during assembly, which suggested that for this capsid disassembly and assembly pathways are not mirror images.[51,53] In other cases, intermediates of the assembly/disassembly reaction were not compared, and microscopic reversibility was not assessed. To sum up, great advances have been made on the understanding of capsid assembly pathways; however, limited experimental information available on assembly pathways of the simplest icosahedral capsids is still hampering detailed comparisons with the predictions of powerful but necessarily simple models and simulations.

In the present study we have enabled and studied in vitro the controlled disassembly and self-assembly under close to physiological conditions of one of the smallest and structurally simplest virus capsids known. The $T = 1$ icosahedral capsid of the parvovirus minute virus of mice (MVM)[57] is only 25 nm in diameter and is made of just 60 structurally equivalent polypeptide subunits[58,59] (Figure 1), an absolute minimum number; there is no quasiequivalence and no conformational switches. During viral infection, the MVM capsid self-assembles in the cell nucleus from just 20 stable trimeric CBBs, which have the shape of an equilateral triangle with a central spike[35,60] (Figure 1). Trimeric CBBs are formed in the cytosol and transported to the cell nucleus, where they associate to form the capsid, without any help from viral scaffolding proteins or the viral nucleic acid (ssDNA), which is later packaged into the preformed (empty) capsid.[57,61] Finally, irreversible maturation of the MVM capsid in vivo is limited to cleavage of the N-terminus of some subunits and occurs only after the capsid has been assembled and the genome has been packaged.

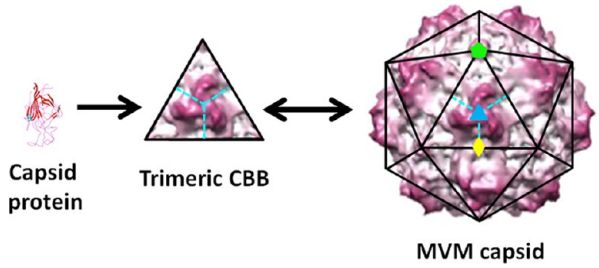

Figure 1. Architecture of the MVM capsid. Three equivalent capsid protein subunits fold and oligomerize to form a stable trimeric CBB in the approximate shape of an equilateral triangle with a large central spike. Twenty CBBs self-assemble to form the icosahedral $T = 1$ capsid. One icosahedral symmetry axis of each type is indicated: triangle, 3-fold; pentagon, 5-fold; diamond, 2-fold.

In summary, the actual architecture of the MVM capsid and the conditions for its in vivo self-assembly resemble most closely the initial assumptions of the simplest models and simulations of capsid self-assembly, which would allow particularly detailed and accurate comparisons between theory and experiment. We have used a combination of transmission EM (TEM) and high-resolution atomic force microscopy (AFM) in single-particle experiments to both morphologically characterize a series of single transient intermediates and quantify their reversible succession during self-assembly and disassembly of the MVM capsid. The experimental results are closely matched by those of molecular dynamics (MD) simulations of icosahedral $T = 1$ capsid self-assembly.

RESULTS

Reversible Disassembly and Reassembly of the MVM Capsid In Vitro. We first set up a method for MVM capsid disassembly and reassembly in vitro and analyzed both reactions by TEM, AFM and SEC as described in detail in the Materials and Methods section included in the Supporting Information (SI). Purified MVM capsids made of 60 identical protein subunits[62] (Figures 2A and 2E) were disassembled at 25 °C in a physiological buffer (phosphate-buffered saline, PBS) containing moderate amounts (typically 3.25−3.5 M) of guanidinium hydrochloride (GdmHCl). The reaction was left to proceed until very few (if any) complete or incomplete capsids remained, as observed by TEM and AFM (Figures 2B and 2F). Comparative SEC analysis before and after GdmHCl treatment (Figure S1 of SI) revealed a shift from a peak corresponding to intact capsids to a peak with a maximum that approximately corresponded to the size of a free CBB (molecular weight 1.95×10^5 Da). The SEC results confirmed the TEM and AFM observations indicating that dissociation was complete and yielded free CBBs.

DOI: 10.1021/jacs.6b07663
J. Am. Chem. Soc. 2016, 138, 15385−15396

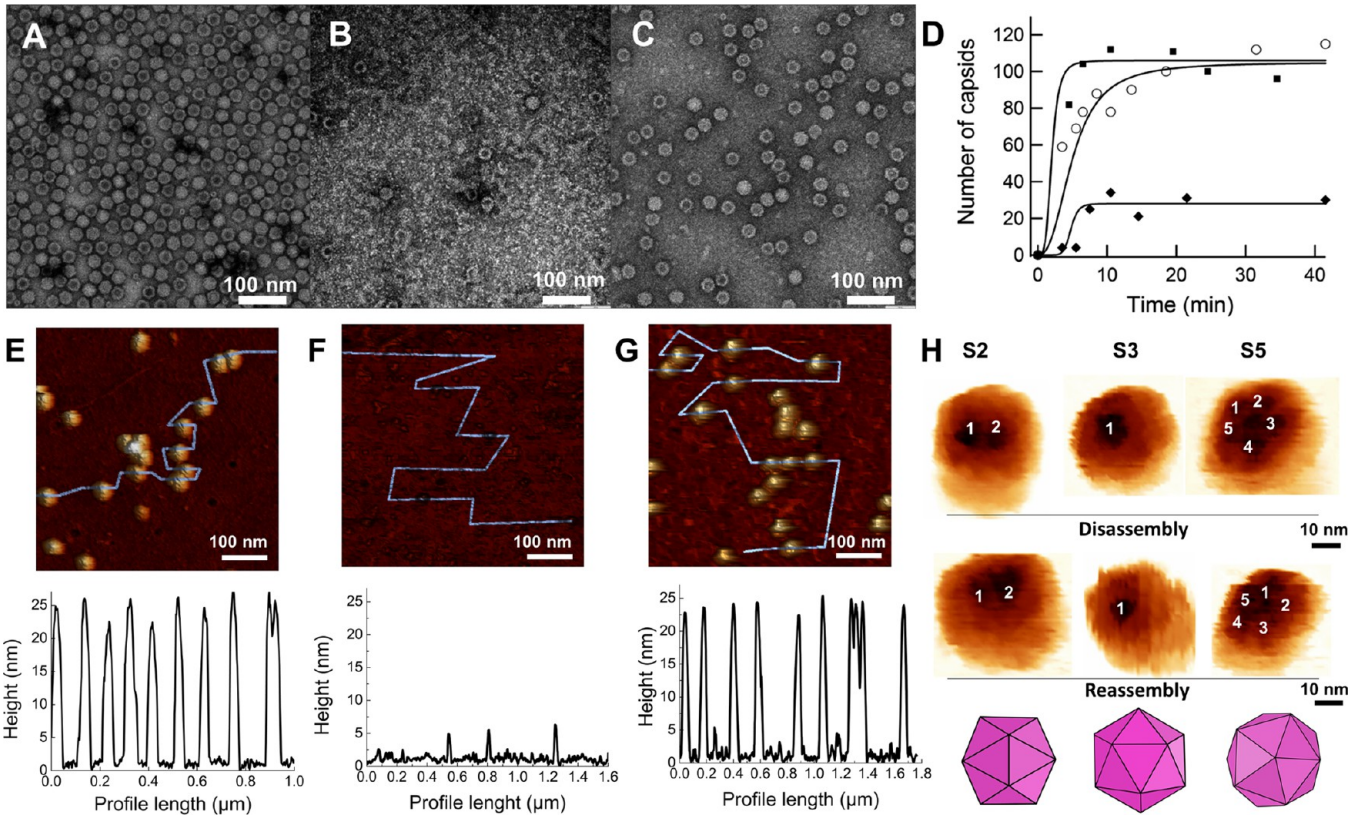

Figure 2. In vitro disassembly and self-reassembly of the MVM capsid. (A–C) Representative TEM images taken at the same magnification and total capsid protein concentration during a typical disassembly and reassembly experiment. (A) Purified capsids. (B) Disassembled capsids from sample imaged in panel (A). (C) Reassembled capsids from sample imaged in panel (B). (D) In vitro self-assembly kinetics of the MVM capsid at different protein concentrations. Closed squares, 0.04 mg/mL; circles, 0.008 mg/mL; diamonds, 0.002 mg/mL. The total number of assembled capsids counted by TEM in 15 random fields of 1.97 μm × 1.97 μm is represented as a function of reaction time. Experimental data were fitted to sigmoidal functions (eq 3 in SI). (E–H) Representative AFM images of purified capsids (E), disassembled capsids (F), or reassembled capsids (G). Concentration of the samples in E, F, G were adjusted to avoid crowding and facilitate the determination of height profiles (below these images). Height profiles correspond to particles encountered along the blue line path in the image. (H) Capsids visualized before disassembly (top images) or after reassembly (bottom images) and oriented with a 2-fold (left), 3-fold (center) or 5-fold (right) symmetry axis close to the top. The corresponding heights ($h_{max} \approx 25$, 26, or 22 nm) matched closely the diameters across the corresponding axes in the atomic model of the MVM capsid determined by crystallography.[59] Icosahedrons in similar orientations are also depicted. Scale bars are included. Objects visualized by AFM appear laterally expanded because of tip-object dilation effects.

After disassembly, the denaturant was immediately removed by dialysis against PBS. At protein concentrations between 0.35 and 1.5 mg/mL, both TEM and AFM imaging repeatedly showed the virtual disappearance of a large part of the capsid-derived small particulate material observed after disassembly (Figures 2B and 2F), and its reassembly into complete capsids (Figures 2C and 2G).

In vitro-reassembled capsids imaged by TEM and AFM at a late point of assembly could not be distinguished from in vivo-assembled capsids in shape, diameter (compare Figures 2A and 2C), height (compare Figures 2E and 2G) or topography (compare Figure 2H). Even at the moderate temperature (25 °C) and low CBB concentrations used, the efficiency of the reassembly process was relatively high (up to ~35%, or higher if aggregated reassembled capsids that were observed in low proportions in some experiments are considered). Reassembly efficiency tended to decrease if the disassembled sample was left in the presence of GdmHCl during enough additional time, probably because of the eventual coupled dissociation and unfolding of the CBBs themselves.[62] Comparative SEC analysis of sample aliquots before assembly and after reassembly in a same experiment yielded a reassembly efficiency similar to that obtained by TEM analysis (data not shown). At the latest time point of the reaction (Figure 2G), 31 out of 33 particles (94%) analyzed by AFM corresponded to complete capsids. These results indicate that MVM capsid (dis)assembly in a physiological buffer is a reversible reaction, which can be displaced toward disassembly or reassembly by simply adding or removing moderate amounts of a chemical denaturant.

The kinetics of capsid reassembly in PBS at different protein concentrations was determined by quickly (≤3 min.) removing the denaturant using a desalting column as described in Materials and Methods (see SI) and counting complete particles in EM images obtained at different reaction times. Under these conditions, some assembly took place even at protein concentrations as low as 0.002 mg/mL (Figure 2D). This result suggests that the critical protein concentration could be <0.03 μM. However, this may not be necessarily the case, as assembly of single spherical viral particles has been observed at concentrations well below the critical concentration.[63] Fitting to sigmoidal kinetics (eq 3 in SI) as expected for a nucleation and growth process revealed a protein concentration-dependent reaction, and a long lag phase at the lowest concentrations tested (Figure 2D). For spherical particles, a lag phase has been

DOI: 10.1021/jacs.6b07663
J. Am. Chem. Soc. 2016, 138, 15385–15396

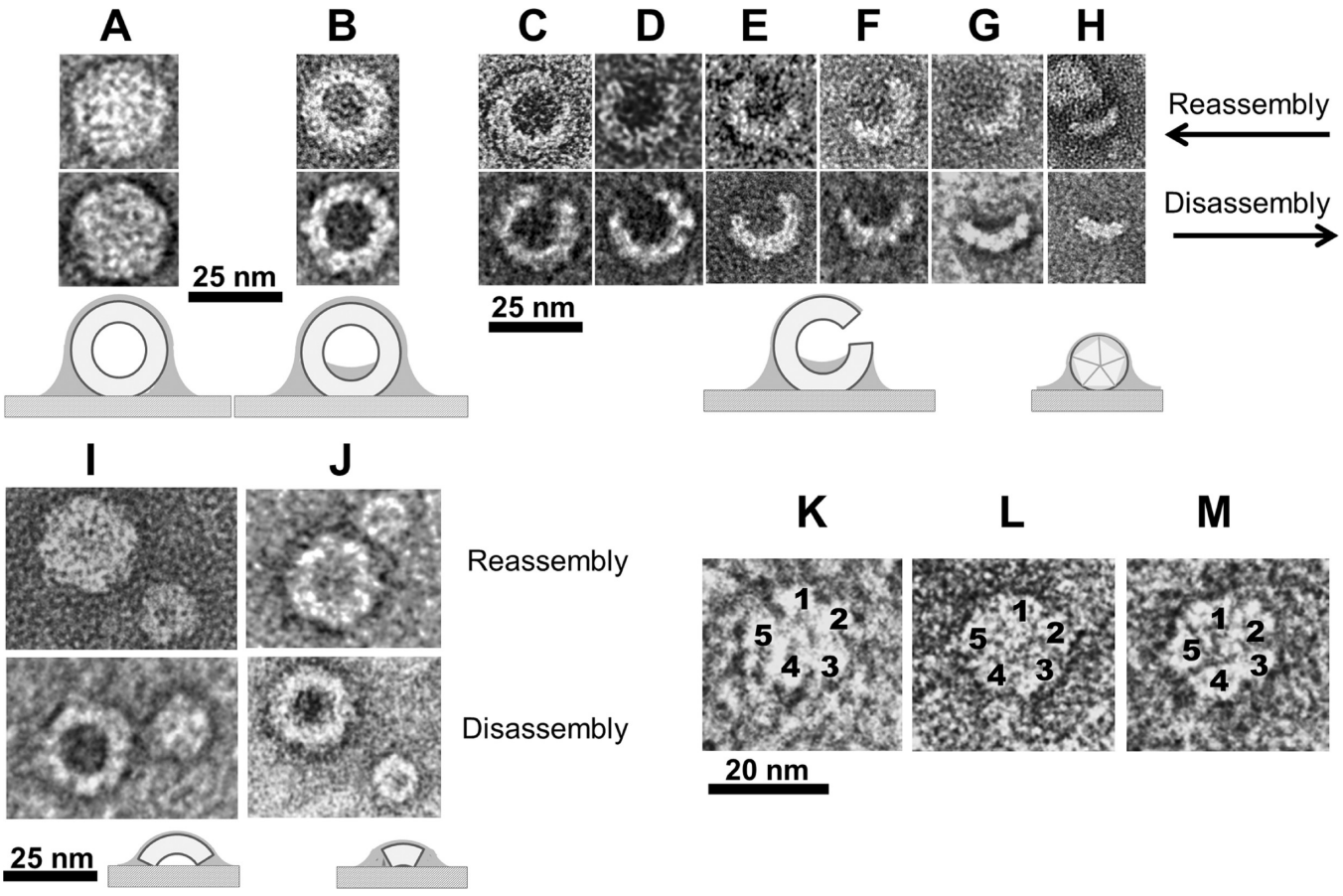

Figure 3. Categorization of different transient intermediates visualized by TEM during disassembly or assembly of the MVM capsid. For each panel from (A) to (J), the intermediates in either top or bottom images were respectively observed during either capsid self-assembly or disassembly, and all are shown at the same scale. Gray shadowing of the schematic particles shown below some TEM images correspond to the idealized distribution of the staining agent (uranyl) in or around each particle type. (A) Type EM_I (complete capsids in a basal state); (B) EM_{II} (complete rearranged capsids); (C–G) EM_{III} (incomplete capsids, from capsids missing one or a few CBB to capsid fragments missing most CBBs), viewed from the side; (H–M) EM_{IV} (small capsid fragments); in panels (I,J), a complete capsid beside the fragment facilitates size comparisons. Fragments in panels H (~18–20 nm wide), I (~18–20 nm in diameter) or J (~9–10 nm in diameter) show dimensions respectively comparable to a pentamer of CBBs viewed either from the side or from the front (or back), and to a single CBB viewed from the front (or back), but identification is uncertain due to limited resolution. (K–M) Higher magnification and resolution TEM images of five-lobed structures detected during disassembly or reassembly experiments that may correspond to pentamers of CBBs. Numbers identify individual CBBs in each pentamer (for a clear identification of pentamers of CBBs see Figure 4).

shown to be proportional to the time it takes to complete the particle and indicative of multistep assembly.[64]

The Reversible Assembly/Disassembly Reaction of the MVM Capsid Proceeds through an Ensemble of Transient Intermediates That Can Be Observed and Characterized. We then attempted to identify and structurally characterize any transient intermediates that could occur during the in vitro disassembly or self-assembly of the MVM capsid. First, different concentrations of GdmHCl were added to purified MVM capsids to try and decrease the difference in free energy, and thus increase the proportion of disassembly intermediates relative to complete capsids and/or free CBBs. Samples were incubated at 25 °C for >60 min, and aliquots were taken at different times and immediately imaged by TEM and/or AFM. At low GdmHCl concentrations (0–0.5 M), only complete capsids were significantly populated, whereas at relatively high GdmHCl concentrations (≥4 M) only capsid-derived small particulate material was observed. Under these conditions (dis)assembly behaved as a two-state reaction.[62] However, at intermediate GdmHCl concentrations (1.5–3.5 M), partially disassembled capsids and capsid fragments were observed in substantial proportions during many minutes, until at the longer times only small particulate material was visible (Figure S2). Based on these results, an intermediate concentration of GdmHCl (3.25 or 3.5 M) was chosen for subsequent experiments. After GdmHCl removal immediately after disassembly was complete, partially reassembled capsids and, given enough time, fully reassembled capsids were observed (Figure S3).

Before attempting any quantification of the relative abundance of the diverse incomplete capsid forms at different times during the (dis)assembly reaction, we carried out their morphological characterization and categorization. We started either with assembled capsids that were disassembled (Figure S2), or with fully disassembled capsids that were then reassembled (Figure S3). High-magnification TEM images (Figure 3) allowed an estimation of sizes and shapes of incomplete capsids and fragments, while high-resolution (<1 nm in height) AFM images (Figure 4) allowed an accurate determination of their heights and the identification of topographic features, which helped in identifying which parts were missing in many single particles.

DOI: 10.1021/jacs.6b07663
J. Am. Chem. Soc. 2016, 138, 15385–15396

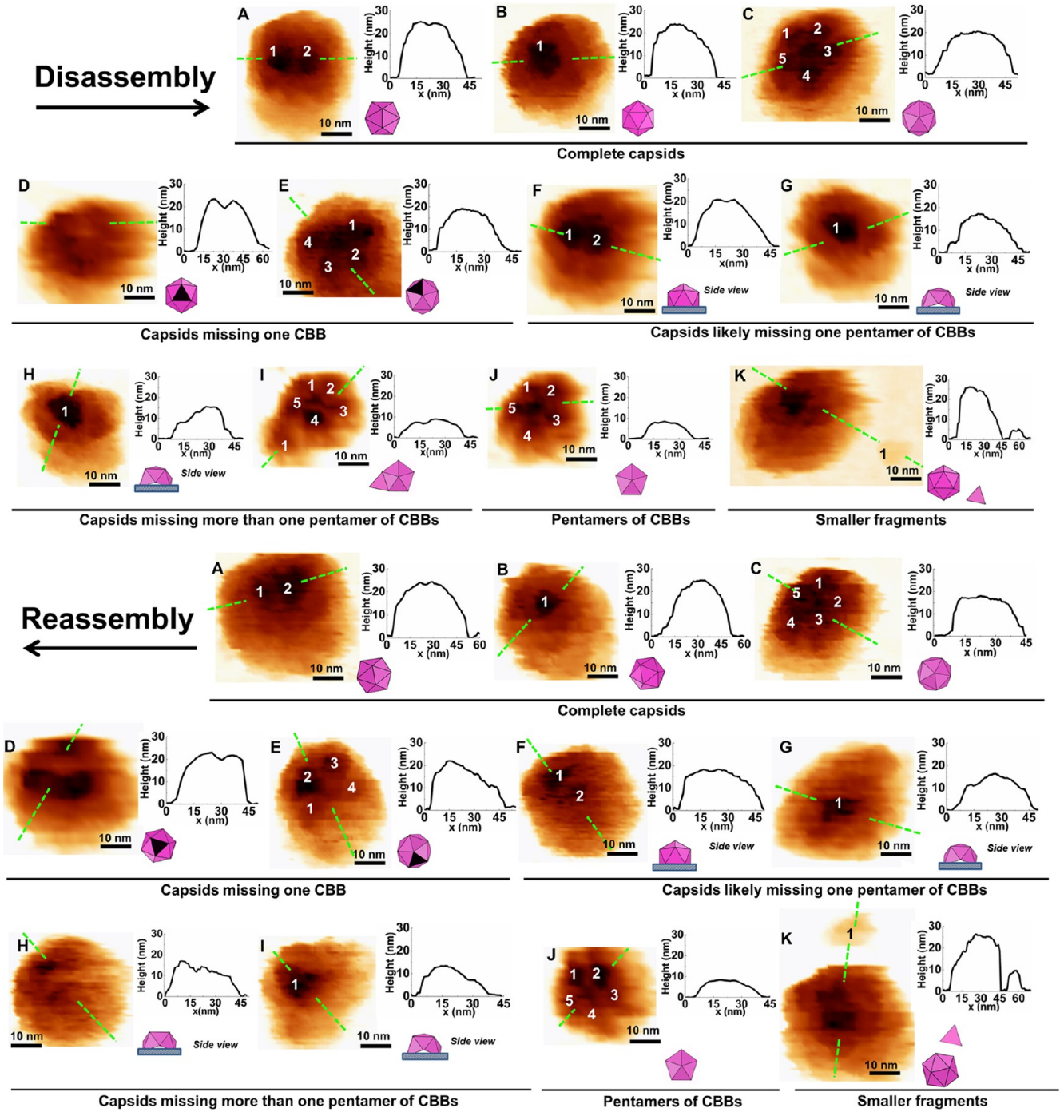

Figure 4. Categorization of different transient intermediates of MVM capsid disassembly (upper half of the figure) or assembly (bottom half) visualized by AFM. In these AFM images, increased height is indicated by darker tones. (A,B,C) Complete capsids in different orientations; (D,E) Incomplete capsids missing one CBB; (F,G) Incomplete capsids that may be missing one pentamer of CBBs, or a similar number of subunits from one side of the particle. (H,I) Incomplete capsids missing larger fragments; (J) An isolated pentamer of CBBs; (K) A small fragment with a height similar to that of a single CBB (labeled 1), beside a complete capsid. In some images, the large spikes located at the center of the uppermost CBBs in the viral particle are indicated with numbers. All images are represented at the same scale. At right from each imaged particle, its height profile obtained by following the dotted green line is indicated. Below each height profile, a scheme of the icosahedral particle is included to facilitate interpretation of particle orientation and which parts appear to be missing. These schemes are represented in the same top view as the corresponding particles imaged by AFM, except in some cases in which, for clarity, a side view of the model that may represent the particle lying on the solid substrate (gray horizontal bar) is shown.

Assembly and Disassembly Intermediates Imaged by TEM. Figure 3 shows representative images of the diverse viral particles and capsid fragments observed by TEM during both disassembly and self-assembly experiments.

The MVM particles observed by TEM were categorized as follows: In intact capsid samples kept in close to physiological conditions, nearly all particles were of either type EM_I (Figure 3A) or EM_{II} (Figure 3B), with a diameter of ~25 nm. These types correspond to two known conformational states of the

DOI: 10.1021/jacs.6b07663
J. Am. Chem. Soc. 2016, 138, 15385−15396

intact MVM capsid.[57,61,62,65] In the basal state (EM_I), the pores located at the 12 5-fold symmetry axes are not large[58,59] and conformationally dynamic enough to allow through-pore translocation events;[57,61,62,65] in this state, the capsid would be also impervious to uranyl ions. However, it is known that both in vivo and in vitro the MVM capsid may change its conformation under external stimuli (e.g., by moderate heating or addition of low GdmHCl concentrations in vitro).[62] This conformational change, which may lead to the capsid adopting the EM_{II} state, enables biologically relevant through-pore translocation events,[62,65] and may also facilitate penetration of uranyl ions.[66] Moderate heating of the evolutionarily related canine parvovirus capsid similarly led to increased uptake of the staining agent NanoW.[67] The possibility that EM_{II} particles correspond instead to capsids missing one or several CBBs can be ruled out by additional evidence: MVM virion preparations, in which the nucleic acid fills the particles and sterically prevents entry of uranyl ions, contained only EM_I particles, while capsid preparations obtained using a similar protocol invariably contained similar proportions of EM_I and EM_{II} particles and virtually no other particle types. High-resolution AFM imaging of 82 single capsids from a same preparation containing ~40% EM_I and ~60% EM_{II} particles did not reveal missing CBBs in any of them; it also yielded a unimodal, narrow Gaussian distribution of particle heights, with average maximum height $h_{max} \approx 25.3 \pm 1.5$ nm (Figure S4), which accurately corresponds to the average diameter of the intact capsid obtained by X-ray crystallography.[58,59] By contrast, when incomplete capsids were actually present (i.e., during disassembly experiments, see below), missing CBBs and/or significantly reduced heights were clearly detected for many of the particles. To conclude, EM_{II} particles correspond to rearranged complete capsids that have taken uranyl ions through conformationally more dynamic pores or other transient openings.

Both during capsid disassembly using moderate concentrations of denaturant and during self-assembly in a physiological buffer, complete capsids (EM_I and EM_{II}) and many incomplete capsid forms (categorized within either type EM_{III} or EM_{IV}) were present in sizable numbers (Figure 3). Type EM_{III} particles (Figures 3C−H) correspond to incomplete capsids in which a part is missing in one side of the particle (see scheme below images 3E-F). We observed a full series of these incomplete particles during both disassembly and reassembly; all of them had the same radius of curvature of complete capsids (~12 nm), but lacked increasingly larger fragments. This series of incomplete capsid forms could be expected if trimeric CBBs were sequentially removed from the MVM capsid during its disassembly, and added during the self-assembly reaction to form the complete capsid. Small arc-shaped fragments (Figure 3H) have the same size, radius of curvature and subtended angle of a pentamer of trimeric CBBs (a quarter capsid) if viewed from the side (scheme below Figure 3H).

Type EM_{IV} included many roundish particles with diameters ranging from ~10 nm to ~20 nm (Figures 3I−M). These particles were very infrequently or not observed before disassembly was triggered, and must, thus, correspond to small capsid fragments. The largest of these particles (Figure 3I) showed a diameter close to that of a free pentamer of trimeric CBBs seen from either the front or back; a pentagonal symmetry could be discerned by TEM at higher magnification and resolution (Figures 3K−M). Many of the abundant, smaller roundish particles that could still be individualized in TEM images (Figure 3J) showed diameters that were comparable to that of a CBB, although the resolution was not high enough to discern the shape of particles as small as free CBBs. Further support for these structural interpretations of EM_I to EM_{IV} particles observed by TEM was provided by height profiles and topographic features determined by high-resolution AFM imaging (next).

Intermediates Imaged by AFM. The samples containing partially disassembled capsids that had been imaged by TEM were also imaged by AFM in a liquid, using PBS buffer to approach physiological conditions of pH and ionic strength as described in Materials and Methods (see SI). AFM images taken just before disassembly showed many complete capsids ($h_{max} \approx 25$ nm; Figure S5A), and only a few very small particles ($h_{max} \approx 5$ nm; see below). In contrast, images taken at long incubation times (e.g., 360 min, Figure S5B) showed very few complete capsids and a heterogeneous mixture of many smaller particles (22 nm> $h_{max} \geq 5$ nm), indicative of intermediate forms from nearly complete capsids to small fragments showing a size and height similar to those of individual CBBs.

The architectures of different capsid subassemblies observed during disassembly or assembly were then analyzed using high-resolution AFM imaging (Figure 4).

The larger particles (Figure 4A-C) corresponded to complete capsids. Many of the incomplete capsids and smaller fragments (22 nm > h_{max} > 8 nm) showed also a characteristic topography with a 5-fold, 2-fold or 3-fold axis close to the top (Figures 4D−J). Height profiles combined with topographic analysis indicated the presence of the following subassemblies: (i) incomplete capsids missing one CBB only (Figure 4D,E); (ii) capsids that may be missing one pentamer of CBBs or a similar number of subunits (Figure 4F,G); (iii) capsids missing larger parts (Figure 4H,I); (iv) free pentamers of CBBs (quarter capsids) (Figure 4J); and (v) smaller fragments, with a large number of particles showing a $h_{max} \approx 5$ nm, the height of a free CBB adsorbed flat on the surface (Figure 4K shows one of these particles, labeled "1", beside a complete capsid). The imaged intermediates could be imaged again in a second scan without any structural alteration being detected. We did not observe incomplete capsids showing more than a single "hole" in the particle, but a second fragment could be missing at the underside of the particle. To sum up, the results of high-resolution AFM analysis (Figure 4) supported and extended the structural interpretations for both disassembly and assembly intermediates obtained by TEM (Figure 3).

Unproductive Association of Incomplete Capsids and Formation of Aberrant Particles During MVM (Dis)-assembly. Both during disassembly and reassembly, pairs of incomplete capsids missing only minor parts and apparently fused to each other were very occasionally observed by TEM and AFM (Figure S6). This situation may not be generally caused by mere juxtaposition: In those pairs, the incomplete capsids were nearly always observed with their unsatisfied binding interfaces in front of each other. Some of these pairs (Figure 6C) showed a remarkable similarity to the twinned, small $T = 1$ capsids of ssDNA geminiviruses joined at a missing capsomer. Moreover, such associations remained even when partially disassembled capsid samples were highly diluted and the particles were adsorbed at very low densities on glass for AFM imaging (Figure S6D,E).

A few other aberrant assemblies were also very infrequently observed during both self-assembly and disassembly. Partic-

DOI: 10.1021/jacs.6b07663
J. Am. Chem. Soc. 2016, 138, 15385−15396

ularly conspicuous among these rare forms were thin, long filaments (10−12 nm in diameter as determined by height measurements using AFM, and up to several μm in length as determined by TEM) (Figure S7). These observations indicate that during self-assembly of the MVM capsid, and also during its disassembly, off-pathway reassociation events lead to misassembled viral particles. However, their very low occurrency under close to physiological conditions revealed a remarkably faithful self-assembly process.

A Size-Dependent Progression of Intermediates during MVM Capsid Assembly and Disassembly. The above results revealed that MVM capsid assembly is an essentially reversible reaction, with the same kinds of intermediates being observed during assembly or disassembly (Figures 3 and 4). We proceeded next to independently estimate by TEM and AFM the kinetics of appearance and/or disappearance of different transient intermediates and end products during both the assembly pathway and the disassembly pathway, and compared the results.

First, MVM capsids were disassembled at 25 °C in the presence of GdmHCl, and the kinetics of appearance and/or disappearance of each of different categories of particles were quantified by taking aliquots at different times, immediate imaging by TEM and/or AFM, and counting large numbers of particles in many random imaged fields to provide statistically significant results. It was important to avoid overinterpretation by considering the individual kinetics of too many categories of intermediates with no clearly defined boundaries between them. Thus, for kinetic analysis we operationally grouped the many different particles visualized into only a few categories, depending on the technique used (either TEM or AFM), as described next.

Disassembly Kinetics and Pathway Followed by TEM. Highly purified MVM capsid samples were incubated at 25 °C in the presence of 3.25 M GdmHCl for different amounts of time. The particles were grouped as indicated above (Figure 3), but type EM_{III} was divided into two subtypes representing larger or smaller incomplete capsids: EM_{IIIA}, incomplete capsids that lost less than half of the CBBs (Figures 3C−D), and EM_{IIIB}, incomplete capsids that lost between half and three-quarters of the CBBs (Figures 3E−G). EM_{IV} particles (with dimensions that correspond to pentamers of CBBs or trimeric CBBs) were too small and (at the longer times) too numerous to be counted by TEM. The results of a detailed, representative experiment are shown in Figure 5A and Table S1. Repetition of the experiment yielded the same conclusions.

EM_I complete capsids in basal state decreased with time, with a best fit of the decay curve that corresponds to two exponential decay processes (eq 2 in SI): one very fast (estimated rate constant k_{EMId1} = 1.34 min^{-1}), and the other slower (k_{EMId2} = 0.02 min^{-1}). EM_{II} complete capsids in a rearranged state first increased in numbers and later decreased; the data could be best fitted to the sum of a very fast exponential formation process (k_{EMIIa} = 0.53 min^{-1}), and a slower exponential decay (k_{EMIId} = 0.03 min^{-1}). A simplest interpretation of these results is that, under those conditions, the capsid basal state is rapidly converted into the conformationally rearranged state at a rate given by $k_{EMId} = k_{EMIIa}$ (around 1 min^{-1}, averaged from the two values obtained, and within the error of these values); and both capsid forms are independently disassembled at a similar rate, given by $k_{EMId2} = k_{EMIId}$ (around 0.02−0.03 min^{-1}). The kinetic results indicate that EM_I capsids can be directly disassembled without necessarily being converted into EM_{II} capsids; EM_{II} capsids are not obligatory disassembly (or assembly) intermediates.

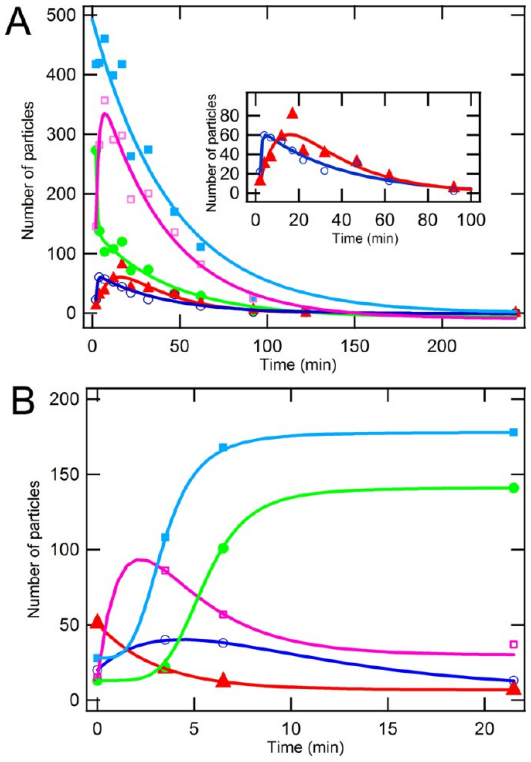

Figure 5. A reciprocal progression of intermediates during disassembly or assembly of the MVM capsid, as determined by TEM. The results of typical disassembly (A) or reassembly (B) experiments are shown. The total number of different types of particles counted by TEM in 15 random fields of 0.49 μm × 0.49 μm (A) or 12 random fields of 0.98 μm × 0.98 μm (B) under controlled conditions are represented as a function of reaction time. Light blue squares, types EM_I + EM_{II} particles (complete capsids); green circles, EM_I (complete capsids in basal state); magenta open squares, EM_{II} (complete rearranged capsids); blue open circles, EM_{IIIA} (large incomplete capsids); red triangles, EM_{IIIB} (smaller incomplete capsids). The standard deviations obtained when the number of capsid particles per field were averaged provide evidence for the representativity of the fields used for counting particles. For example, for complete capsids in panel A, the averages ± standard deviations obtained for 15 fields counted for each time point from 2 to 242 min were: 28 ± 7; 28 ± 9; 31 ± 8; 27 ± 3; 28 ± 7; 18 ± 4; 18 ± 4; 11 ± 4; 7 ± 2; 2 ± 2; 0 ± 0; 0 ± 0. For each particle type, fitting to a single exponential, a double exponential or a sigmoidal process, as indicated in the text (eqs 1−3 in SI), is represented by a colored line. For the assembly process, the limited number of data points allowed an apparently good fitting, but rate constants thus obtained are unreliable and have not been included in Table S1. The inset graph in panel A facilitates comparison of the appearance and disappearance of EM_{IIIA} and EM_{IIIB} incomplete capsids during capsid disassembly.

Incomplete capsids (EM_{IIIA} and EM_{IIIB}) increased in numbers at relatively short times ($k_{EMIIIAa}$ = 1.38 min^{-1}; $k_{EMIIIBa}$ = 0.11 min^{-1}) and then decreased at longer times ($k_{EMIIIAd}$ = 0.03 min^{-1}; $k_{EMIIIBd}$ = 0.04 min^{-1}). The time at which a maximum number of EM_{IIIA} or EM_{IIIB} incomplete capsids was reached was inversely proportional to their sizes, with larger incomplete capsids (between nearly complete capsid and half-capsid) peaking first and smaller incomplete capsids (between half-capsid and quarter-capsid) peaking later (Figure 5A).

DOI: 10.1021/jacs.6b07663
J. Am. Chem. Soc. 2016, 138, 15385−15396

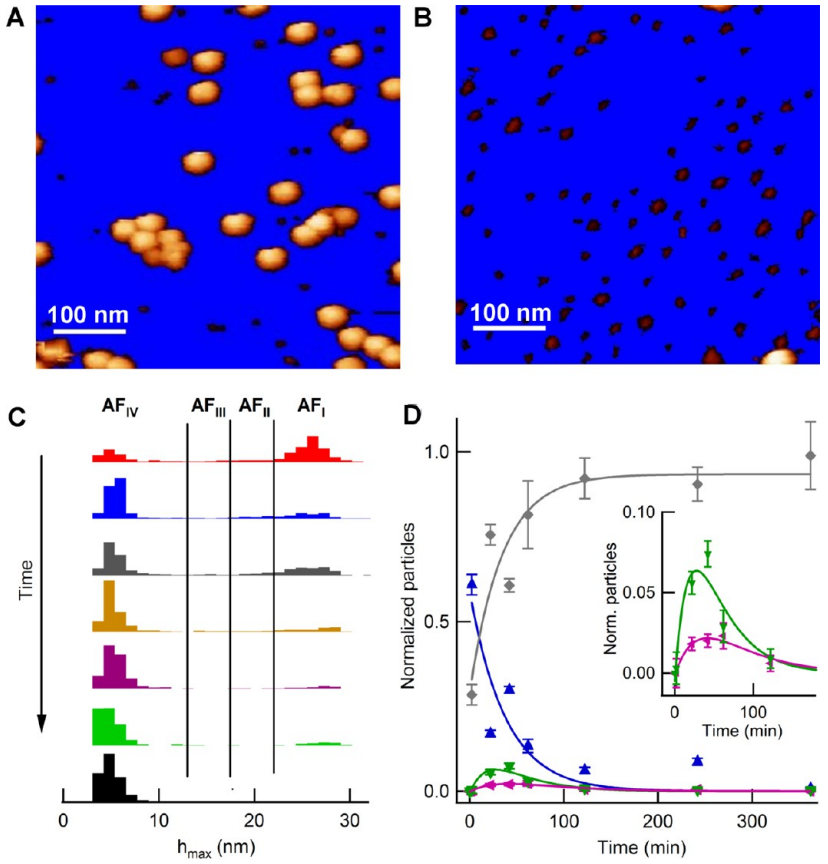

Figure 6. A progression of intermediates during disassembly of the MVM capsid, as determined by AFM. The results of a typical disassembly experiment are shown. 59 fields of 0.5 μm × 0.5 μm were counted. (A,B) Representative fields imaged by AFM at the beginning (A) or end (362 min) (B) of the reaction. (C) Histograms representing the number of particles as a function of h_{max} of the particle, at different disassembly times (top to bottom: 2, 22, 42, 62, 122, 242, and 362 min); a close-up of the central part of the histograms is shown in Figure S8. The number of particles of different h_{max} in 6 to 12 fields per time point were counted by automated *Flooding* analysis and the data processed as detailed in Supporting Information. Each histogram has been normalized relative to the total number of particles automatically counted (between 40 and 120 particles, depending on the time point). The vertical lines across the histograms define the limits used to categorize the particles into four types (AF_I to AF_{IV}) according to h_{max}. A near-continuum of incomplete capsids of different height was observed; the cutoff between AF_{II} and AF_{III} was arbitrarily chosen only to be able to determine whether smaller incomplete capsids tended to appear later than larger incomplete capsids. (D) The fraction of particles of different types is represented as a function of reaction time. Blue triangles, type AF_I particles (h_{max} > 22 nm, complete capsids); green inverted triangles, AF_{II} (h_{max} = 17.5−22 nm, large incomplete capsids); magenta triangles, AF_{III} (h_{max} = 13−17.5 nm, smaller incomplete capsids); gray diamonds, AF_{IV} (h_{max} = 3.6−13 nm, smaller capsid fragments). At the longer times (242 and 362 min) the AF_{IV} fraction respectively reached 90.51% and 98.87%; at these two times the respective proportions of other particle types were AF_I: 8.72% and 0.85%; AF_{II}: 0.26% and 0.28%; AF_{III}: 0.51% and 0%. Standard errors were calculated from the individual histograms obtained by counting particles of each type in each imaged field and are indicated for each data point. Color lines correspond to fitting curves to either single or double exponential processes, as described in the text (eqs 1 or 2 in SI). The inset graph facilitates comparison of the appearance and disappearance of AF_{II} and AF_{III} incomplete capsids during capsid disassembly.

Disassembly Kinetics and Pathway Followed by AFM. Automated height profiling and counting of many complete or incomplete capsids in many AFM scans provided a second, independent method to quantify the relative abundance and formation and/or decay rate constants of different particle types during (dis)assembly of the MVM capsid. In addition, it allowed an estimation of the appearance of very small capsid fragments that could not be reliably counted by TEM. The results obtained by AFM in a disassembly experiment are shown in Figure 6 and Table S1.

Type AF_I (complete capsids, h_{max} > 22 nm) yielded a disassembly rate of k_{AFId} = 0.03 min^{-1}. AF_{II} (larger incomplete capsids; h_{max} = 17.5−22 nm) first increased in numbers (k_{AFIIa} = 0.05 min^{-1}) and later decreased (k_{AFIId} = 0.03 min^{-1}). Type AF_{III} (smaller incomplete capsids; h_{max} = 13−17.5 nm) first increased in number (k_{AFIIIa} = 0.03 min^{-1}) and later decreased (k_{AFIIId} = 0.02 min^{-1}). As also observed by TEM, larger incomplete capsids (type AF_{II}) peaked first and smaller incomplete capsids (type AF_{III}) peaked somewhat later. Smaller capsid fragments (type AF_{IV}, h_{max} = 3.6−13 nm), including pentamers of CBBs and free CBBs) rapidly increased in numbers and reached a plateau at the longest reaction times analyzed (>150 min) (k_{AFIVa} = 0.03 min^{-1}).

There is no correspondence between the operationally defined categories of particle types based on either TEM (shape, diameter) or AFM (height, topography) visualization. Thus, the rate constants and other quantitative parameters obtained by TEM or AFM cannot be generally compared because they do not refer to equivalent categories of intermediates. Even so, the results obtained by the two approaches are remarkably consistent. For example, the rate constant for disappearance of complete capsids (types EM_I +

DOI: 10.1021/jacs.6b07663
J. Am. Chem. Soc. 2016, 138, 15385−15396

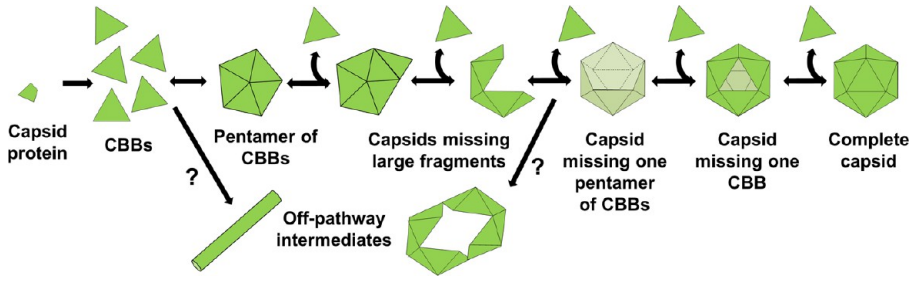

Figure 7. A schematic experiment-derived model for self-assembly of the simple $T = 1$ MVM capsid. Stable trimeric CBBs reversibly assemble into pentamers of CBBs. Capsid assembly then proceeds through a cascade of reversible reactions, in which trimeric CBBs are added one at a time. Capsids lacking one pentamer of CBBs (shown in a lighter shade) may be intermediates, but their existence has not been fully established. In the last stages of assembly, capsids lacking just one CBB are observed. Very infrequently, off-pathway intermediates are formed. Question marks indicate that the branching off points leading to the observed off-pathway intermediates are only educated guesses. See text for a detailed description.

EM_{II} by TEM, type AF_I by AFM) was quite consistent (Table S1) when it was respectively determined by TEM or AFM at similar denaturant concentrations.

Self-Assembly Kinetics and Pathway. The kinetics of appearance and/or disappearance of each of different types of incomplete or complete MVM capsids (EM_I, EM_{II}, EM_{IIIA} and EM_{IIIB}) during reassembly in physiological conditions of pH and ionic strength was quantified by TEM as we had done in disassembly experiments. Data were fitted to sigmoidal growth curves (complete capsids) and/or exponential formation/decay curves (intermediates) (eqs 1−3 in SI). Due to the speed with which assembly intermediates appeared and disappeared, data collection could be done only at a quite limited number of time points before the process was essentially complete, and kinetic parameters could not be reliably determined. However, the results obtained (Figure 5B) did reveal that (i) smaller incomplete capsids (EM_{IIIB}, containing between one-quarter and one-half of the CBBs in the complete capsid) peaked first, while larger incomplete capsids (EM_{IIIA}, containing more than half of the CBBs in the complete capsid) peaked later; (ii) complete capsids in the more dynamic state (EM_{II}) first increased in number and later decreased upon their conversion into complete capsids in the basal state; (iii) complete capsids in the basal state (EM_I) rapidly increased in number after a short lag phase, and approached a plateau after ∼10 min. These results indicated that the succession of transient intermediates observed during the self-assembly pathway of the MVM capsid may mirror the succession of intermediates observed during the disassembly pathway.

DISCUSSION

An Empirical Model of the Self-Assembly Pathway of a Simplest $T = 1$ Icosahedral Virus Capsid. In this combined single-particle TEM-AFM study, transient intermediates during the reversible self-assembly of one of the simplest ($T = 1$) icosahedral virus capsids known have been experimentally singled out, imaged to high resolution, structurally characterized and quantified. Efficient self-assembly of the MVM capsid was achieved at physiological pH and ionic strength. Moreover, the reaction mimicked the conditions of assembly in the cell nucleus in vivo, in which this capsid is formed from just 20 stable trimeric CBBs without any conformational switches imposed by quasiequivalence, and without intervention of scaffolding proteins or the viral nucleic acid.[35,60] As a consequence, the results obtained here for the assembly process contribute to the experimental verification under close to physiological conditions of detailed predictions of theoretical studies on assembly intermediates and pathways of the simplest ($T = 1$) virus capsids; they also provide a framework from which current self-assembly models and simulations for viral capsids and other nanoparticles could be refined and expanded.

The results presented in Figure 2 revealed that (i) self-assembly of the $T = 1$ MVM capsid in vitro presents the signatures of an efficient nucleation and growth process that depends strongly on CBB concentration; (ii) fairly high yields of complete capsids (up to at least 35%) could be obtained; (iii) under some conditions some assembly occurred even at very low protein concentrations (0.03 μM), although the critical concentration could be higher;[63] (iv) the lag phase indicates that even the few capsids assembled at the lowest concentrations are the result of nucleation in a multistep process,[64] and not of growth from a few, not fully disassembled capsid fragments that could be present at the start of the reaction.

Single-particle structural characterization and quantification of assembly and disassembly intermediates by TEM and AFM as described here provide support for an experiment-based model for the reversible self-assembly pathway of a $T = 1$ icosahedral capsid (Figure 7):

(i) Trimers of capsid subunits act as preformed, stable CBBs in MVM,[35,60] and probably also in related parvoviruses;[68] (ii) pentamers of CBBs constitute conspicuous early intermediates; (iii) trimeric CBBs are sequentially joined, leading to gradual capsid growth and a continuous series of incomplete capsid intermediates differing in just one trimeric CBB; (iv) pentamers of CBBs and incomplete capsids occur only in small proportions and peak at fairly short times during the assembly process; (v) smaller incomplete capsids containing less CBBs peak at shorter times compared to larger incomplete capsids containing more CBBs, as expected if they are on-pathway intermediates (and not off-pathway assemblies that must partially dissociate before yielding complete capsids); (vi) in incomplete capsids, only neighboring subunits appear to be missing, leading to a single "hole" in the particle; (vii) conspicuous, relatively stabilized assembly intermediates as characterized by high-resolution AFM include pentamers of CBBs, incomplete, three-quarter capsids lacking one pentamer of CBBs or a similar number of CBBs, and incomplete capsids lacking just one CBB; (viii) at the end of the assembly process, no significant numbers of intermediate-size aggregates remain; (ix) the same types of intermediates occur in reverse during both disassembly and reassembly of the MVM capsid; the times at which incomplete capsids of different sizes are more

DOI: 10.1021/jacs.6b07663
J. Am. Chem. Soc. 2016, 138, 15385−15396

abundant are consistent with the disassembly and assembly pathways being mirror images from each other. Thus, the principle of microscopic reversibility[69] may apply to the self-assembly/disassembly reaction of a simple virus capsid; (x) aberrant particles occur only infrequently during both self-assembly and disassembly, which supports the high efficiency of the process under biologically relevant conditions. The fact that these misassembled particles are also observed during disassembly underscores the reversibility of the process.

Comparison with MD Simulations and Theoretical Models. Both Rapaport[28,30,31] and Brooks and associates[27] used coarse-grained MD simulations to explore the reversible self-assembly pathway, in the presence of solvent, of a generic $T = 1$ capsid from just 20 triangular capsomers (CBBs) in the absence of conformational switches, scaffolding proteins and the viral nucleic acid. As mentioned above, these simple conditions correspond precisely to those encountered in the actual process of self-assembly of the $T = 1$ MVM capsid both in vivo and in vitro.

The model that emerged from the simulations by Rapaport on a $T = 1$ capsid from 20 CBBs[28,30,31] included, among others, the following features: (i) self-assembly consists of a cascade of reversible stages, with a strong preference for low-energy intermediate states, including pentamers of CBBs; (ii) the process efficiently leads to complete capsids, without leaving many incomplete capsids or producing many aberrant assemblies; (iii) analysis of assembly pathways for individual capsids indicates that growth to pentamer size is generally rapid; (iv) during assembly, a substantial fraction of events involves the release of subunits, emphasizing the reversible nature of the process; (v) pentamers of CBBs (5-mer) and capsids lacking one CBB only (19-mer) are less prone to losing subunits than other subassemblies; (vi) in growing capsids, losses or additions of 1 CBB account for the majority of events, but those involving 5 CBBs (as in a pentamer) had an increased likelihood compared to other sizes; (vii) partially assembled capsids had a tendency to present few discontinuities, showing a minimal number of openings; (viii) incorrect assemblies through merging of incomplete capsids were sometimes observed; (ix) assembled capsids were stable even at capsid subunit concentrations where assembly did not occur, indicating hysteresis of dissociation; this phenomenon had been first predicted in the thermodynamic-kinetic model by Zlotnick and associates and experimentally verified (using $T > 1$ capsids): during the early stages of dissociation, capsids that lack just one CBB accumulate transiently and create a barrier for further dissociation, acting like a kinetic trap.[70]

Brooks and associates[27] used also coarse-grained MD simulations to develop a geometric model of the self-assembly pathway of a $T = 1$ capsid made of 20 triangular CBBs, but without enforcing specific assembly rules. Their model included the following features: (i) sigmoidal kinetics and other features indicate a nucleation and growth process; (ii) formation of different structures, including incomplete and complete capsids and off-pathway aggregates, depends strongly on CBB concentration. Under optimum conditions: (iii) assembly becomes highly efficient; (iv) capsid growth proceeds by adding one CBB at a time and not by collapse of previously formed, large oligomers; (v) small CBB oligomers, and even larger intermediates, exist only in small amounts over short periods of time early in the simulations; (vi) at the end of the simulations no intermediate-size aggregates remain; (vii) lifetimes of nearly complete capsids are larger than those of smaller incomplete capsids, and addition of the last CBB to 19-mer incomplete capsids is rate-limiting, probably due to entropic considerations; (viii) misassembled structures formed at low frequency under nonoptimal conditions include merged incomplete capsids.

Comparison between the empirical model of $T = 1$ icosahedral capsid self-assembly derived from the present study (described above), and the remarkable predictions of these MD simulations for a generic $T = 1$ capsid reveals a very good general agreement. This agreement is extended to many particular details, as can be appreciated from the similarity of most of the above-mentioned specific features of the empirical model and the simulations. Thus, the experimental results on self-assembly and disassembly of the MVM capsid obtained in this study verify to a fine level of detail the predictions derived from coarse-grained MD simulations of assembly of the simplest icosahedral capsids. In addition, those experimental results provide constraints to develop further refined models and simulations of icosahedral capsid self-assembly, that could be tested in detail by using the in vitro self-assembly system set up in this study. Finally, comparison with both theoretical predictions and experimental results obtained on the assembly of more complex icosahedral capsids by Zlotnick and other researchers (see the Introduction) reveals that many previous conclusions on icosahedral capsid self-assembly can be extended to even the simplest ($T = 1$) capsids under biologically relevant conditions.

AFM as a Powerful Technique to Visualize at High Resolution and Automatically Quantify Assembly and Disassembly Intermediates. Adsorption to a solid substrate (silanized glass) of MVM capsids and assembly/disassembly intermediates for AFM imaging in a physiological buffer had no detected effects on their structure, and they were not significantly deformed either. The heights of intact capsids measured along the three types of symmetry axes accurately matched the diameters determined by X-ray crystallography along the corresponding axes. Moreover, adsorbed particles, including complete capsids, incomplete capsids or capsid fragments, remained stable over substantial periods of time and could be imaged more than once without noticing any structural changes. Only after purposeful application of enough mechanical force through the AFM tip could MVM capsids and virions be partially disrupted.[71] Comparison for a $T = 1$ capsid of assembly intermediates predicted by MD simulations that did not consider mechanical force,[27,28,30,31] disassembly and self-assembly intermediates formed in bulk solution (this study) and incomplete capsid particles obtained under mechanical force[71] indicates that, when enough energy is applied to a simple icosahedral virus capsid, either vectorially by mechanical indentation or nonvectorially by other physical or chemical means, the same weakest protein−protein interfaces are disrupted.

To sum up, from a technical point of view the present study shows that AFM, with its access to the vertical dimension of single nanoparticles, can be combined with conventional TEM imaging in a powerful approach to structurally characterize with remarkable resolution the transient intermediates of supramolecular self-assembly and disassembly processes in solution, even under biologically relevant conditions. Moreover, it demonstrated that automated methods to analyze AFM images can be used to quantify intermediates and obtain kinetic parameters of reactions involving the (dis)assembly of virus capsids or other nanoparticles in solution.

DOI: 10.1021/jacs.6b07663
J. Am. Chem. Soc. 2016, 138, 15385−15396

The In Vitro Self-Assembled MVM Capsid for Nanotechnological Applications. The MVM capsid presents remarkable properties and biological functions that make it an excellent choice for developing different biomedical and nanotechnological applications.[35,57,62,65,72,73] Moreover, its architectural simplicity and the abundant biophysical, biochemical and biological knowledge acquired on MVM facilitate its engineering by genetic and/or chemical techniques to better suit different applications.[72,74] The efficient, faithful self-assembly of the MVM capsid in vitro under quite simple conditions, as set up in this study, enables a simple in vitro approach to encapsidate drugs and nanomaterials[8,13,15,16,19] in this particularly useful virus-based nanoparticle.

■ ASSOCIATED CONTENT

Supporting Information

The Supporting Information is available free of charge on the ACS Publications website at DOI: 10.1021/jacs.6b07663.

Supporting Methods, Figures S1−S8, and Table S1 (PDF)

■ AUTHOR INFORMATION

Corresponding Author

*mgarcia@cbm.csic.es

ORCID

Mauricio G. Mateu: 0000-0002-2915-1529

Notes

The authors declare no competing financial interest.

■ ACKNOWLEDGMENTS

We gratefully acknowledge D. Reguera for critical reading of the manuscript. We thank M.T. Rejas and M. Guerra, J.I. Belio and J.A. Pérez for technical help with EM and figures, respectively. M.M. and A.V. are the respective recipients of a FPI fellowship from Universidad Autónoma de Madrid and a postdoctoral contract from the Spanish Ministerio de Economía y Competitividad (MINECO). M.G.M. is an associate member of the Institute for Biocomputation and Physics of Complex Systems, Zaragoza, Spain. This work was funded by grants from MINECO/FEDER EU (BIO2012-37649 and BIO2015-69928-R) and by an institutional grant from Fundación Ramón Areces.

■ REFERENCES

(1) Porterfield, J. F.; Zlotnick, A. In *Physical Virology*; Stockley, P. G., Twarock, R., Eds.; Imperial College Press: London, U.K., 2010; pp 131−158.
(2) Zlotnick, A.; Fane, B. A. In *Structural Virology*; Agbandje-McKenna, M., McKenna, R., Eds.; Royal Society of Chemistry Publishing: Cambridge, U.K., 2011; pp 180−202.
(3) Luque, A.; Reguera, D. In *Structure and Physics of Viruses*; Mateu, M. G., Ed.; Springer: Dordrecht, the Netherlands, 2013; pp 553−595.
(4) Mateu, M. G. *Arch. Biochem. Biophys.* **2013**, *531*, 65−79.
(5) Perlmutter, J. D.; Hagan, M. F. *Annu. Rev. Phys. Chem.* **2014**, *66*, 217−239.
(6) Prevelige, P. E., Jr. *Trends Biotechnol.* **1998**, *16*, 61−65.
(7) Zlotnick, A.; Mukhopadhyay, S. *Trends Microbiol.* **2011**, *19*, 14−23.
(8) Douglas, T.; Young, M. *Science* **2006**, *312*, 873−875.
(9) Roy, P.; Noad, R. *Hum. Vaccines* **2008**, *4*, 5−8.
(10) Mateu, M. G. *Protein Eng., Des. Sel.* **2011**, *24*, 53−63.
(11) Yildiz, I.; Shukia, S.; Steinmetz, N. F. *Curr. Opin. Biotechnol.* **2011**, *22*, 901−908.
(12) Glasgow, J.; Tullman-Ercek, D. *Appl. Microbiol. Biotechnol.* **2014**, *98*, 5847−5858.
(13) Li, F.; Wang, Q. *Small* **2014**, *2*, 230−245.
(14) Seeman, N. C.; Belcher, A. M. *Proc. Natl. Acad. Sci. U. S. A.* **2002**, *99*, 6451−6455.
(15) DuFort, C. C.; Dragnea, B. *Annu. Rev. Phys. Chem.* **2010**, *61*, 323−344.
(16) Lee, S.-Y.; Lim, J.-S.; Harris, M. T. *Biotechnol. Bioeng.* **2012**, *109*, 16−30.
(17) *Protein Nanotechnology*, 2nd ed.; Gerrard, J. A., Ed.; Humana Press: New York, 2013; *Methods Mol. Biol.* Vol. *996*.
(18) Wegst, U. G.; Bai, H.; Saiz, E.; Tomsia, A. P.; Ritchie, R. O. *Nat. Mater.* **2015**, *14*, 23−36.
(19) Putri, R.; Cornelissen, J. J.; Koay, M. S. *ChemPhysChem* **2015**, *16*, 911−8.
(20) Zlotnick, A. *J. Mol. Biol.* **1994**, *241*, 59−67.
(21) Schwartz, R.; Shor, P. W.; Prevelige, P. E., Jr.; Berger, B. *Biophys. J.* **1998**, *75*, 2626−2636.
(22) Reddy, V. S.; Giesing, H. A.; Morton, R. T.; Kumar, A.; Post, C. B.; Brooks, C. L., III; Johnson, J. E. *Biophys. J.* **1998**, *74*, 546−558.
(23) Endres, D.; Zlotnick, A. *Biophys. J.* **2002**, *83*, 1217−1230.
(24) Bruinsma, R. F.; Gelbart, W. M.; Reguera, D.; Rudnick, J.; Zandi, R. *Phys. Rev. Lett.* **2003**, *90*, 248101.
(25) Reddy, V. S.; Johnson, J. E. *Adv. Virus Res.* **2005**, *64*, 45−68.
(26) Zandi, R.; van der Schoot, P.; Reguera, D.; Kegel, W.; Reiss, H. *Biophys. J.* **2006**, *90*, 1939−1948.
(27) Nguyen, H. D.; Reddy, V. S.; Brooks, C. L., III *Nano Lett.* **2007**, *7*, 338−344.
(28) Rapaport, D. C. *Phys. Rev. Lett.* **2008**, *101*, 186101.
(29) Katen, S.; Zlotnick, A. *Methods Enzymol.* **2009**, *455*, 395−417.
(30) Rapaport, D. C. *J. Phys.: Condens. Matter* **2010**, *22*, 104115.
(31) Rapaport, D. C. *Phys. Biol.* **2010**, *7*, 045001.
(32) Hagan, M. F. *Adv. Chem. Phys.* **2014**, *155*, 1−68.
(33) Bancroft, J. B.; Hills, G. J.; Markham, R. *Virology* **1967**, *31*, 354−379.
(34) Bancroft, J. B. *Adv. Virus Res.* **1970**, *19*, 99−134.
(35) Almendral, J. M. In *Structure and Physics of Viruses*; Mateu, M. G., Ed.; Springer: Dordrecht, the Netherlands, 2013; pp 307−328.
(36) Sorger, P. K.; Stockley, P. G.; Harrison, S. C. *J. Mol. Biol.* **1986**, *191*, 639−658.
(37) Berthet-Colominas, C.; Cuillel, M.; Koch, M. H. J.; Vachette, P.; Jacrot, B. *Eur. Biophys. J.* **1987**, *15*, 159−168.
(38) Prevelige, P. E., Jr.; Thomas, D.; King, J. *Biophys. J.* **1993**, *64*, 824−835.
(39) Zlotnick, A.; Johnson, J. M.; Wingfield, P. W.; Stahl, S. J.; Endres, D. *Biochemistry* **1999**, *38*, 14644−14652.
(40) Zlotnick, A.; Aldrich, R.; Johnson, J. M.; Ceres, P.; Young, M. J. *Virology* **2000**, *277*, 450−456.
(41) Parent, K. N.; Doyle, S. M.; Anderson, E.; Teschke, C. M. *Virology* **2005**, *340*, 33−45.
(42) Tuma, R.; Tsuruta, H.; French, K. H.; Prevelige, P. E., Jr. *J. Mol. Biol.* **2008**, *381*, 1395−1406.
(43) Morton, V. L.; Stockley, P. G.; Stonehouse, N. J.; Ashcroft, A. E. *Mass Spectrom. Rev.* **2008**, *27*, 575−595.
(44) Knapman, T. W.; Morton, V. L.; Stonehouse, N. J.; Stockley, P. G.; Ashcroft, A. E. *Rapid Commun. Mass Spectrom.* **2010**, *24*, 3033−3041.
(45) Teschke, C. M.; Parent, K. N. *Virology* **2010**, *401*, 119−130.
(46) Shoemaker, G. K.; van Duijn, E.; Crawford, S. E.; Uetrecht, C.; Baclayon, M.; Roos, W. H.; Wuite, G. J. L.; Estes, M. K.; Prasad, B. V. V.; Heck, A. J. *Mol. Cell. Proteomics* **2010**, *9*, 1742−1751.
(47) Uetrecht, C.; Barbu, I. M.; Shoemaker, G. K.; van Duijn, E.; Heck, A. J. *Nat. Chem.* **2011**, *3*, 126−132.
(48) Gordon, E. B.; Knuff, C. J.; Fane, B. A. *J. Virol.* **2012**, *86*, 9911−9918.
(49) Tresset, G.; Le Coeur, C.; Bryche, J.-F.; Tatou, M.; Zeghal, M.; Charpilienne, A.; Poncet, D.; Constantin, D.; Bressanelli, S. *J. Am. Chem. Soc.* **2013**, *135*, 15373−15381.

DOI: 10.1021/jacs.6b07663
J. Am. Chem. Soc. 2016, 138, 15385−15396

(50) Pierson, E. E.; Keifer, D. Z.; Selzer, L.; Lee, L. S.; Contino, N. C.; Wang, J.C.-Y.; Zlotnick, A.; Jarrold, M. F. *J. Am. Chem. Soc.* **2014**, *136*, 3536−3541.
(51) Law-Hine, D.; Sahoo, A. K.; Bailleux, V.; Zeghal, M.; Prevost, S.; Maiti, P. K.; Bressanelli, S.; Constantin, D.; Tresset, G. J. *J. Phys. Chem. Lett.* **2015**, *6*, 3471−3476.
(52) Garmann, R. F.; Comas-Garcia, M.; Knobler, C. M.; Gelbart, W. M. *Acc. Chem. Res.* **2016**, *49*, 48−55.
(53) Law-Hine, D.; Zeghal, M.; Bressanelli, S.; Constantin, D.; Tresset, G. *Soft Matter* **2016**, *12*, 6728−6736.
(54) Steinbach, S.; Wistuba, A.; Bock, T.; Kleinschmidt, J. A. *J. Gen. Virol.* **1997**, *78*, 1453−1462.
(55) Sánchez-Rodríguez, S. P.; Münch-Anguiano, L.; Echeverría, O.; Vázquez-Nin, G. M.; Mora-Pale, M.; Dordick, J. S.; Bustos-Jaimes, I. *Biochimie* **2012**, *94*, 870−878.
(56) Xu, J.; Guo, H.-C.; Wei, Y.-Q.; Dong, H.; Han, S.-C.; Ao, D.; Sun, D.-H.; Wang, H.-M.; Cao, S.-Z.; Sun, S.-Q. *Appl. Microbiol. Biotechnol.* **2014**, *98*, 3529−3538.
(57) Cotmore, S. F.; Tattersall, P. *Annu. Rev. Virol.* **2014**, *1*, 517−537.
(58) Agbandje-McKenna, M.; Llamas-Saiz, A. L.; Wang, F.; Tattersall, P.; Rossmann, M. G. *Structure* **1998**, *6*, 1369−1381.
(59) Kontou, M.; Govindasamy, L.; Nam, H. J.; Bryant, N.; Llamas-Saiz, A. L.; Foces-Foces, C.; Hernando, E.; Rubio, M. P.; McKenna, R.; Almendral, J. M.; Agbandje-McKenna, M. *J. Virol.* **2005**, *79*, 10931−10943.
(60) Riolobos, L.; Reguera, J.; Mateu, M. G.; Almendral, J. M. *J. Mol. Biol.* **2006**, *357*, 1026−1038.
(61) Plevka, P.; Hafenstein, S.; Li, L.; D'Abramo, A., Jr.; Cotmore, S. F.; Rossmann, M. G.; Tattersall, P. *J. Virol.* **2011**, *85*, 4822−4827.
(62) Carreira, A.; Menéndez, M.; Reguera, J.; Almendral, J. M.; Mateu, M. G. *J. Biol. Chem.* **2004**, *279*, 6517−6525.
(63) Harms, Z. D.; Selzer, L.; Zlotnick, A.; Jacobson, S. C. *ACS Nano* **2015**, *9*, 9087−9096.
(64) Hagan, M. F.; Elrad, O. M. *Biophys. J.* **2010**, *98*, 1065−1074.
(65) Hernando, E.; Llamas-Saiz, A. L.; Foces-Foces, C.; McKenna, R.; Portman, I.; Agbandje-McKenna, M.; Almendral, J. M. *Virology* **2000**, *267*, 299−309.
(66) Goldsmith, C. S.; Miller, S. E. *Clin. Microbiol. Rev.* **2009**, *22*, 552−563.
(67) Nelson, C. D. S.; Minkkinen, E.; Bergkvist, M.; Hoelzer, K.; Fisher, M.; Bothner, B.; Parrish, C. R. *J. Virol.* **2008**, *82*, 10397−10407.
(68) Yuan, W.; Parrish, C. R. *Virology* **2001**, *279*, 546−557.
(69) Fersht, A. R. *Structure and Mechanism in Protein Science*; Freeman: New York, 1999.
(70) Singh, S.; Zlotnick, A. *J. Biol. Chem.* **2003**, *278*, 18249−18255.
(71) Castellanos, M.; Pérez, R.; Carrillo, P. J. P.; de Pablo, P. J.; Mateu, M. G. *Biophys. J.* **2012**, *102*, 2615−2624.
(72) Castellanos, M.; Pérez, R.; Carrasco, C.; Hernando-Pérez, M.; Gómez-Herrero, J.; de Pablo, P. J.; Mateu, M. G. *Proc. Natl. Acad. Sci. U. S. A.* **2012**, *109*, 12028−12033.
(73) Mateu, M. G. *Virus Res.* **2012**, *168*, 1−22.
(74) Mateu, M. G. *Adv. Exp. Med. Biol.* **2016**, *940*, 83−120.

DOI: 10.1021/jacs.6b07663
J. Am. Chem. Soc. 2016, 138, 15385−15396